THE JOURNAL OF PHYSICAL CHEMISTRY Letters

Letter

pubs.acs.org/JPCL

Photochemical Dynamics of Ethylene Cation $C_2H_4^+$

Baptiste Joalland,[†] Toshifumi Mori,[‡,§] Todd J. Martínez,*[,‡] and Arthur G. Suits*[,†]

[†]Department of Chemistry, Wayne State University, Detroit, Michigan 48202, United States

[‡]PULSE Institute and Department of Chemistry, Stanford University, Stanford, California 94305, United States

Supporting Information

ABSTRACT: We present a theoretical study of the nonadiabatic effects in ethylene cation $C_2H_4^+$, the simplest π radical cation, after photoexcitation to its three lowest doublet excited states. Two families of conical intersections are found, with minimum energy structures characterized by planar and twisted geometries. Ab initio multiple spawning dynamical calculations suggest that the competition between these relaxation pathways depends strongly on the initial excited state, with excited state lifetimes in the 30−60 fs range. Ultrafast decay via planar geometries deposits the molecule near a bridged minimum on the ground state, allowing prompt H migration events. The alternative pathway mediated by torsional motion induces important backspawned population transfer promoted by hindered rotations. The results allow us to revisit earlier vibrationally-mediated photodissociation experiments and shed light on the electronic relaxation dynamics of a prototypical radical cation subject to strong vibronic interactions.

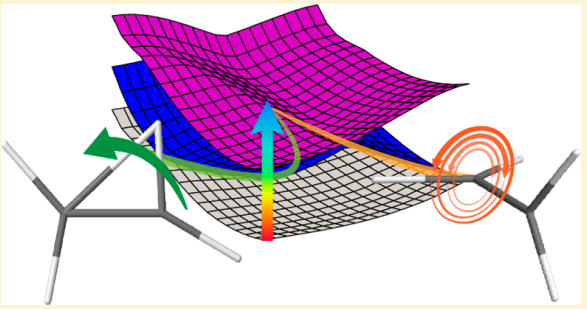

SECTION: Spectroscopy, Photochemistry, and Excited States

The ethylene cation $C_2H_4^+$ is, along with the isoelectronic neutral vinyl C_2H_3, the simplest organic π radical system: one electron populates a unique π orbital in the ground state electronic configuration. The three lowest doublet excited states of $C_2H_4^+$ result from $\sigma \rightarrow \pi$ excitations, and lead to a complex manifold of moderate oscillator strength transitions below the bright $\pi\pi^*$ state. This rich electronic structure motivated pioneering theoretical calculations 30 years ago that established the broad features of the photodynamics of $C_2H_4^+$,[1,2] but advances in theoretical methods and computational power along with recent experimental results[3−6] urge a reinvestigation that can now include nonadiabatic dynamics.

The equilibrium geometry of the ground state cation is a D_2 twisted geometry. From the analysis of vibronic progressions in photoelectron spectra, the torsional angle was first determined to be $27 \pm 2°$ and the torsional barrier 270 ± 150 cm^{-1}.[7] Willitsch et al. recently refined these values to a torsional angle of 29.2° and a torsional barrier of 357 ± 29 cm^{-1} using the high-resolution pulsed-field-ionization zero-kinetic-energy method.[3] These experiments have suggested that the molecular symmetry may be regarded as D_{2h} rather than D_2 due to intense even peaks in the progression of the torsional mode. This is because the zero-point energy (ZPE) in the torsional mode exceeds the torsional barrier at planarity. The molecule therefore undergoes large amplitude torsional motions associated with strong vibronic couplings.[3]

The thresholds for H and H_2 elimination from the ground state are nearly identical:[8]

$$C_2H_4^+ \rightarrow C_2H_2^+ + H_2 \qquad 2.62 \text{ eV}$$

$$C_2H_4^+ \rightarrow C_2H_3^+ + H \qquad 2.70 \text{ eV}$$

Thus, one can expect these dissociation pathways to compete, and the branching ratio between them could provide insights into the complex couplings among the electronic states accessible at modest excitation energies.[9−11] Vibrationally-mediated photodissociation experiments have shown that the excitation of one or two quanta of ν_4, the vibrational mode responsible for twisting the CH_2 moieties, can indeed affect the H/H_2 loss ratio.[4,5]

In order to better understand the photodynamics of $C_2H_4^+$, we carried out simulations using the ab initio multiple spawning (AIMS) method,[12,13] which has been developed to simulate nonadiabatic events on excited electronic states. Forces and nonadiabatic couplings were calculated on-the-fly using the state-averaged complete active space self-consistent field (CASSCF) method[14] with active spaces including 11 electrons and a set of σ, π, and π^* orbitals (SA3-CASSCF(11/8) and SA4-CASSCF(11/7)) (see Supporting Information for more details on the active space choices). All calculations were done with the 6-311G** basis set. The nuclear wavepacket was treated as a superposition of complex frozen Gaussian trajectory basis functions (TBFs, whose centers are propagated classically), and the nonadiabatic coupling vectors were used to decide the time and momenta of spawning events, as has been discussed previously.[15] Minima, transition states, and minimum energy conical intersections (MECIs) were optimized at the above cited levels and also using the extended multistate complete active space second-order

Received: February 18, 2014
Accepted: April 4, 2014
Published: April 4, 2014

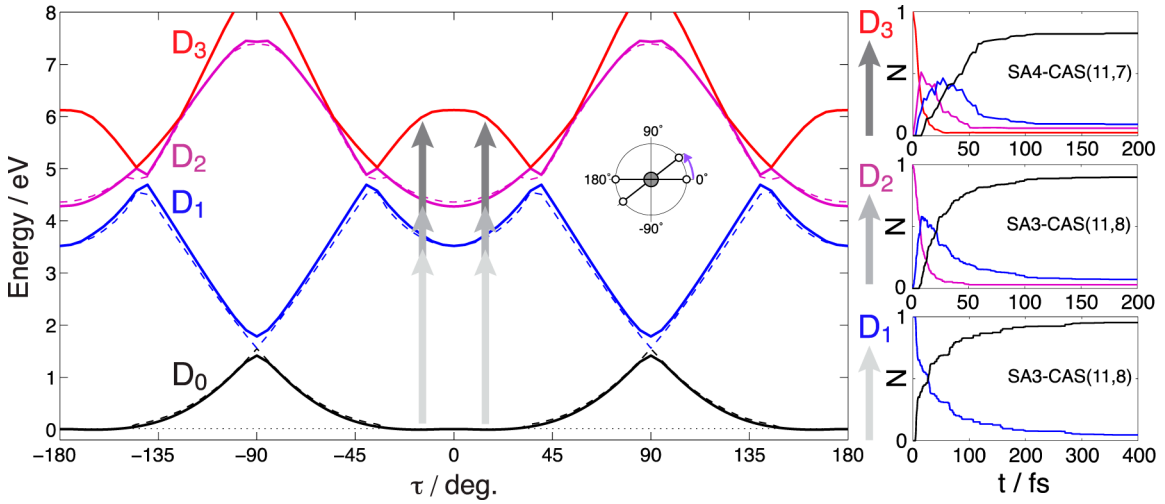

Figure 1. (Left) Potential energy surfaces of adiabatic ground state D_0 (black), D_1 (blue), D_2 (purple), and D_3 (red) along the torsional coordinate calculated at the CASSCF level with the two active spaces used in the AIMS simulations (SA3-CAS(11/8) in dashed lines and SA4-CAS(11/7) in solid lines). The torsion angle τ is defined as the dihedral angle between the two planes formed by the CH_2 moieties, which is the only constrained coordinate while the energy is minimized on D_0. (Right) Time evolution of the populations on each adiabatic state for excitation to D_1 (bottom), D_2 (middle), or D_3 (top).

perturbation theory (XMS-SA4-CASPT2(11/7)) that explicitly treats dynamical electron correlation.[16]

Relaxed torsional scans of the ground and low-lying excited state potential energy surfaces are shown in Figure 1. The torsional barrier at $\tau = 0°$ on D_0 is almost undetectable since it is so small (0.001 and 0.009 eV at the SA3-CAS(11/8) and SA4-CAS(11/7) levels, respectively, to be compared to 0.060 eV at the SA4-CASPT2(11/7) level). A set of avoided crossings around $\tau = 30°$ couple all the $\sigma\pi$ excited states (D_1, D_2, and D_3) to each other. The D_1/D_0 intersection at 90° results from the Jahn–Teller couplings occurring near D_{2d} symmetry.[17] Transition dipole moments for excitations to the $\sigma\pi$ states are strongly dependent on the torsional angle. For $\tau = 0°$, only the $D_0 \rightarrow D_2$ transition is allowed, although intense photoelectron bands (i.e., by exciting the planar neutral system) have been detected for all $\sigma \rightarrow \pi$ transitions. In the present study, photoexcitation to the D_1, D_2, and D_3 states was studied with initial conditions sampled from a Wigner distribution generated from the structure and harmonic frequencies of the cationic ground state global minimum optimized with MP2/6-311**. Under these conditions, excitation to D_3 is strongly optically allowed, while excitation to D_1 is only weakly allowed (cf. Table 1, which summarizes excited state character at the Franck–Condon point). Nearly 50 initial TBFs were prepared and run independently for excitation to D_1 and D_2, and 25 for excitation to D_3. The initial absolute torsional angle $|\tau_i|$ was equal to 18° on average. After spawning, the simulations comprise more than 600 TBFs.

Table 1. Transition Dipole Moment *d*, Franck–Condon (FC) Energies, and Excited State Lifetime $t_{1/2}$ for Excitations to D_1, D_2, and D_3[a]

electronic state	*d* (D)	FC energy (eV)	$t_{1/2}$ (fs)
D_1	2.5×10^{-5} *1.8 × 10⁻⁵*	3.56 *3.57*	43
D_2	0.12 *0.12*	4.43 *4.30*	37
D_3	*0.53*	*6.01*	56

[a]SA3-CASSCF(11/8) (regular) and SA4-CASSCF(11/7) (italic) values were calculated from the cationic D_0 minimum optimized with MP2/6-311**. $t_{1/2}$ is determined by a single exponential fit of the total population on the excited states.

Besides the degenerate double well of the H_2CCH_2 ethylene structure, which constitutes the ground state global minimum of the $C_2H_4^+$ system, Lorquet and co-workers proposed that the isomerization to an ethylidene minimum, with a H_3CCH arrangement similar to its neutral counterpart, precedes the dissociation leading to H_2 loss.[1,2] In our calculations, only a bridged structure, i.e., with a proton bridging the CC bond, is found as another minimum, thus confirming earlier multireference ab initio studies which concluded that an ethylidene-like structure is not stable.[18,19] At the SA4-CASPT2(11/7) level, the bridged structure lies 1.11 eV above the global minimum; both are separated by a transition state TS1 located near the bridged structure at only 1.17 eV (cf. Figure 2 where energetics with ZPE corrections is also shown). The ethylidene geometry is associated with a transition state TS2 located at 1.20 eV that connects hydrogen-bridged structures, which differ by the hydrogen labels (more details on the structures can be found in Supporting Information).

The time evolution of the different populations on each adiabatic state is shown in Figure 1. Regardless of the initially populated electronic state (D_1, D_2, D_3), more than half of the population is transferred to the ground state within 50 fs. Figure 2 shows the structures of the MECIs involved in nonadiabatic transitions, calculated with CASPT2 using the analytic nonadiabatic coupling method introduced previously.[20] We also show the associated population transfers for each of the MECIs, as deduced from the collection of spawning events. We find an unexpected competition between planar and twisted MECIs in the nonadiabatic transitions. Indeed, two D_1/D_0 MECIs, $\mathbf{a_1}$ and $\mathbf{a_2}$, and one for each of the D_2/D_1 and D_3/D_2 transitions constitute a planar relaxation channel, while the torsional relaxation channel is characterized by MECIs **b**. The energies of these key photochemical points optimized at the CASPT2 level are ~0.5 eV lower compared to those resulting from CASSCF optimizations. However, the MECIs D_1/D_0, D_2/D_1, and D_3/D_2 are also accessible at the CASPT2 level from the D_1, D_2, and D_3 Franck–Condon points, respectively. Note that the

dx.doi.org/10.1021/jz500352x | J. Phys. Chem. Lett. 2014, 5, 1467–1471

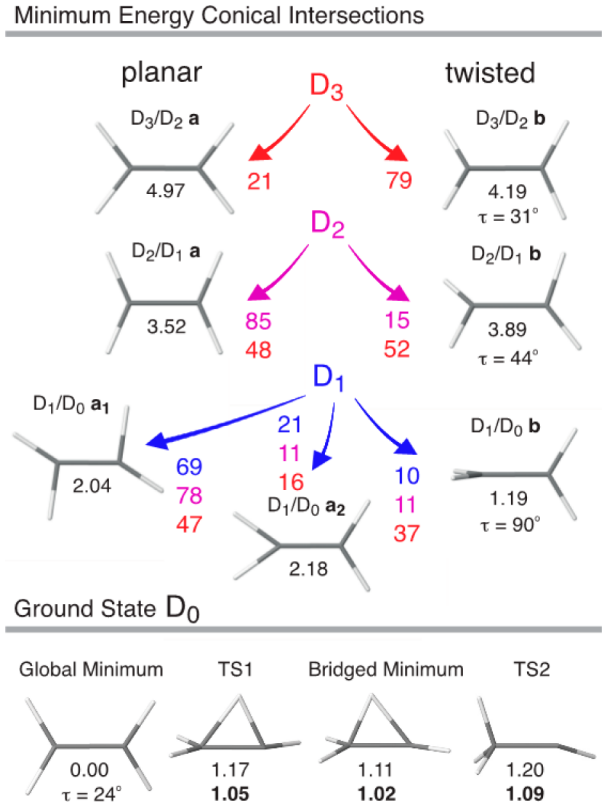

Figure 2. Lower panel: Twisted global minimum, bridged structure, and the two transition states TS1 and TS2 on the ground state D_0. Upper panel: Minimum energy conical intersections and corresponding population transfers (in %) for excitation to D_1 (blue), D_2 (purple), and D_3 (red). Energies (eV) relative to the ground state global minimum are shown, calculated with SA4-CASPT2(11/7). Bold values correspond to energies corrected for ZPE.

D_3/D_2 MECI **b** is a three state intersection (3SI) located along the D_2/D_1 seam, which promotes a rapid series of D_3 to D_2 to D_1 nonadiabatic transitions. Previous theoretical studies on the dynamics around 3SI have highlighted this typical behavior, both in AIMS simulations of full-dimensional molecules[21,22] and also in multiconfiguration time-dependent Hartree[23] (MCTDH) studies of a reduced dimensionality Jahn−Teller model system.[24]

After initial excitation to either D_1 or D_2, the dynamics is dominated by planar D_2/D_1 and D_1/D_0 transitions. Only ∼10% of the initial distribution is observed to decay nonradiatively through twisted conical intersections. In contrast, the competition between nonradiative transitions through planar and twisted pathways is more pronounced after initial excitation to D_3. Twisted geometries dominate the D_3/D_2 transitions (79%) while planar geometries dominate the subsequent D_1/D_0 transitions (∼60%). A splitting of the wavepacket is therefore very effective around the D_2/D_1 twisted CIs in the high-energy region. Nearly 40% of the population transfers to the ground state via the 90° twisted D_1/D_0 CI. No dissociation events have been observed from the excited states, nor any H migrations, although dissociation might be possible with a more flexible wave function (i.e., with a larger active space). Hence, ultrafast nonadiabatic transitions bring the system back to the ground state primarily via the planar D_1/D_0 CI **a1**, which is located near the bridged minimum on D_0. An intuitive photodynamics picture can then be drawn, based on the torsional potential (cf. Figure 1). For excitation to D_1 and D_2, the system relaxes mainly via planar CIs, but can eventually overcome the torsional barrier and decay through the twisted D_1/D_0 CI. For excitation to D_3, the nonadiabatic couplings in the manifold of the D_3/D_2 and D_2/D_1 seams induce wavepacket splitting into two nearly equally populated ground state wavepackets at $\tau = 0°$ and 90°.

To gain further insights into the two main D_1/D_0 transitions, we plot the potential energy surfaces of D_0 and D_1 and their difference $\Delta E_{D0/D1}$ along the torsional and migration coordinates (angle τ and CCH angle φ, respectively) in Figure 3. The planar

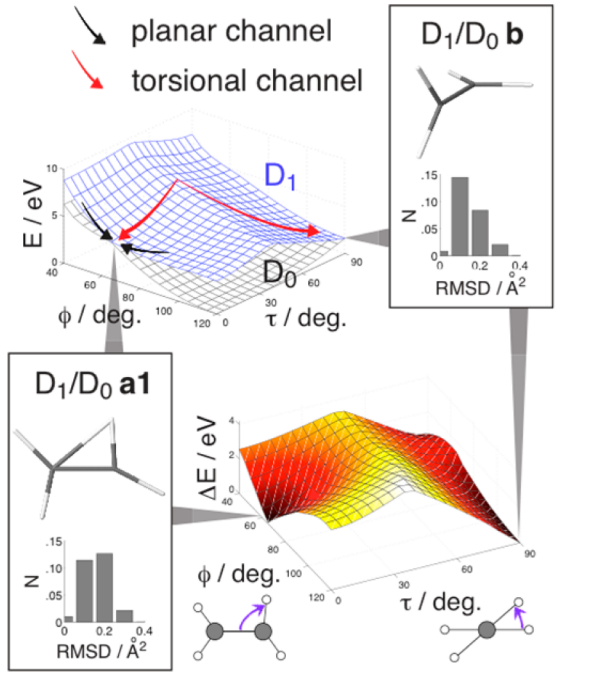

Figure 3. D_0 and D_1 PESs and their difference ΔE [as calculated with SA4-CASSCF(11/7)] are plotted as functions of torsion angle τ and H migration φ coordinates. Insets show the absolute population transferred to D_0 per nonadiabatic transition (spawning event) as a function of the root-mean-square deviation (RMSD) from the D_1/D_0 $\mathbf{a_1}$ and D_1/D_0 **b** MECIs during the nonadiabatic event. These population transfers are averaged over all calculated spawning events. After excitation to D_2, the planar relaxation channel deposits the system near the bridged structure on the ground state (black arrows). For excitation to D_2 and D_3, the $D_3/D_2/D_1$ manifold induces an effective splitting between planar and twisted D_1/D_0 transitions (red arrows). Two typical D_1/D_0 spawning geometries are illustrated in the insets.

D_1/D_0 CI $\mathbf{a_1}$ corresponds to an H migration coordinate of $\varphi \approx 60°$. In contrast, the twisted D_1/D_0 CI **b** exhibits little propensity for H migration, with $\varphi \approx 0°$. The population transfer rates calculated for the whole collection of D_1/D_0 spawning events as a function of the root-mean-square deviation (RMSD) indicate tight transitions, i.e., transitions occurring near the MECI. Both CIs lead to similar population transfers, although the twisted events are slightly tighter.

Two typical D_1/D_0 trajectories involving spawning events near $\tau = 0°$ and 90° are characterized by the time evolution of the population and of the torsional and migration coordinates in Figure 4. No trajectory survives on D_1 near the planar CI after 50 fs. Half CH_2 rotation over the Franck−Condon barrier at $\tau = 90°$ is observed, as well as some prompt H migration events within 50 fs after complete relaxation (indicated by simultaneous low and high CCH angles within the same CH_2 moiety). The CCH angles for each C−H bond are incoherent, and overall the

dx.doi.org/10.1021/jz500352x | J. Phys. Chem. Lett. 2014, 5, 1467−1471

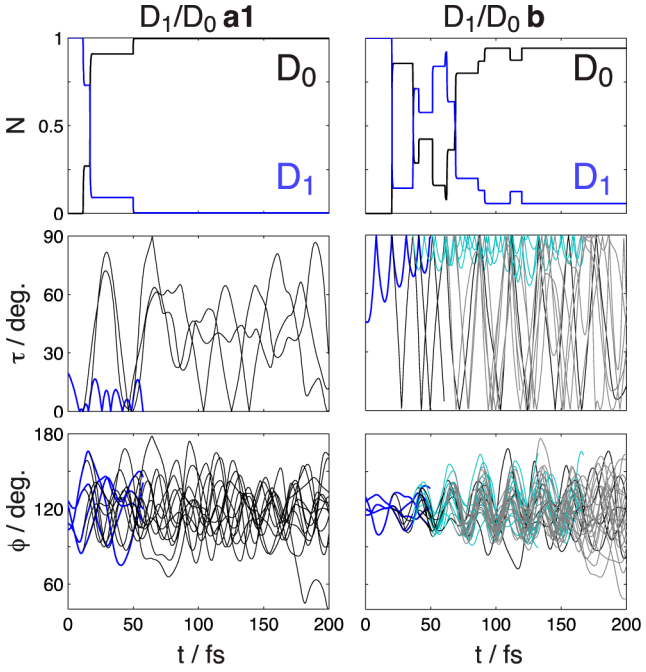

Figure 4. Evolution of representative trajectory basis functions for the first 200 fs after excitation to D_1. The [0−200] fs time evolutions of D_1/D_0 trajectories involving the conical intersections at $\tau = 0°$ (left) and 90° (right) are represented as a function of the torsional τ and migration φ coordinates (all CCH angles, cf. corresponding initial spawning geometries in Figure 3). Initial trajectories on D_1 are represented in blue and D_1 back-spawned children in cyan. Trajectories on D_0 resulting from spawning of the initial D_1 wavepacket are represented in black and the second generation of D_0 trajectories is represented in gray. Accessing the D_1/D_0 CI at $\tau = 0°$ requires a partial migration of H that provokes prompt migration on the ground state (simultaneous CCH angles at 60° and 180°). Strong vibronic couplings associated with CH_2 hindered rotations are observed at $\tau = 90°$.

dynamics suggests that the vibrational energy redistribution is rapidly effective after this type of transition. For the decay at the twisted CI, the initial wavepacket also spawns to the ground state and disappears before 50 fs. The system then undergoes complete CH_2 rotations and creates back-spawned children twice each re-encounter, which correspond to D_0 to D_1 nonadiabatic transitions with transfers to D_1 involving more than 80% of the D_0 population. This significant back-spawning mechanism is repeated for more than 100 fs following successive relaxations to the ground state, and becomes less significant after ∼200 fs (<10%). In the [50−150] fs time window, we observe a near coherent excitation of all the C−H bends for the back-spawned trajectories on D_1, an effect which carries over to the subsequently spawned TBFs on D_0.

These observations raise questions of the possible influence of such dynamics on the unimolecular reaction branching ratios. There are three dissociation channels available, namely $H_2CCH_2^+ \rightarrow C_2H_3^+ + H$, $H_3CCH^+ \rightarrow HCCH^+ + H_2$, $H_3CCH^+ \rightarrow H_2CCH^+ + H$, in addition to the interconversion pathway $H_2CCH_2^+ \rightarrow H_3CCH^+$. The main D_1/D_0 CI $\mathbf{a_1}$ facilitates H migrations and thus brings the molecule closer to H_2 elimination (we associate here the bridged structure to H_3CCH^+). On the other hand, the excitation of the vibrational mode ν_4, which is very anharmonic and strongly decoupled from the other vibrational degrees of freedom, could *prevent* the interconversion to the bridged structure by creating families of hindered rotors with a significant lifetime, in line with the observation of coherent oscillations over several picoseconds associated with vibrational states after ultrafast electronic decay seen in several molecular systems.[25] This sheds light on the H/H_2 ratio previously measured in vibrationally-mediated photodissociation experiments.[5] The threshold observed at internal energy $U = 4.1$ eV, which changes the H/H_2 ratio from nearly 1:1 to 2:1, suggests that a nonstatistical effect is acting in favor of H loss or in disfavor of H_2 loss. The opening of the torsional channel could be responsible for this effect: Below the threshold, the dominant role of the planar relaxation channel ensures significant H_2 losses; above the threshold, the torsional relaxation channel inhibits the randomization over the other vibrational modes and subsequently the interconversion to the bridged structure. This photochemical picture contrasts with the previous one drawn by Lorquet and co-workers, in which the decay to the ground state was proposed to be controlled by a CI corresponding to C−H bond elongation.[2]

This analysis is reminiscent of what was observed earlier in the propanal cation and might be a general feature in radical photoexcitation: the complex and coupled manifold of excited states combined with low thresholds for decomposition on the ground state give rise to nonstatistical decay paths.[26,27] Furthermore, regions where Jahn−Teller interactions are operative, typically located at low altitudes in the potential energy landscape, can experience strong nonequilibrium effects due to the nonadiabatic relaxation from the upper states, as shown here for the prototypical system ethylene cation.

■ ASSOCIATED CONTENT

Supporting Information

Comparative table of transition dipole moments and Franck−Condon energies at the different levels of calculation, as well as Cartesian coordinates of the ground state minima, transition state, and MECIs. This material is available free of charge via the Internet at http://pubs.acs.org.

■ AUTHOR INFORMATION

Corresponding Authors

*E-mail: asuits@wayne.edu.

*E-mail: todd.martinez@stanford.edu.

Present Address

[§](T.M.) Institute for Molecular Science, Okazaki, Aichi 444-8585, Japan.

Notes

The authors declare no competing financial interest.

■ ACKNOWLEDGMENTS

The National Science Foundation has funded this work under award number CHE-1111348. The authors thank Christian Evenhuis, Pascal Krause, and Myung-Hwa Kim for helpful discussions and comments on the manuscript.

■ REFERENCES

(1) Lorquet, J.; Sannen, C.; Raseev, G. Dissociation of the Ethylene Cation: Mechanism of Energy Randomization. *J. Am. Chem. Soc.* **1980**, *102* (27), 7976−7977.

(2) Sannen, C.; Raşeev, G.; Galloy, C.; Fauville, G.; Lorquet, J. Unimolecular Decay Paths of Electronically Excited Species. II. The $C_2H_4^+$ Ion. *J. Chem. Phys.* **1981**, *74*, 2402−2411.

(3) Willitsch, S.; Hollenstein, U.; Merkt, F. Ionization from a Double Bond: Rovibronic Photoionization Dynamics of Ethylene, Large Amplitude Torsional Motion and Vibronic Coupling in the Ground State of $C_2H_4^+$. *J. Chem. Phys.* **2004**, *120*, 1761−1774.

(4) Kim, M. H.; Leskiw, B. D.; Suits, A. G. Vibrationally Mediated Photodissociation of Ethylene Cation by Reflectron Multimass Velocity Map Imaging. *J. Phys. Chem. A* **2005**, *109* (35), 7839−7842.
(5) Kim, M. H.; Leskiw, B. D.; Shen, L.; Suits, A. G. Vibrationally Mediated Photodissociation of $C_2H_4^+$. *J. Phys. Chem. A* **2007**, *111* (31), 7472−7480.
(6) van Tilborg, J.; Allison, T. K.; Wright, T. W.; Hertlein, M. P.; Falcone, R. W.; Liu, Y.; Merdji, H.; Belkacem, A. Femtosecond Isomerization Dynamics in the Ethylene Cation Measured in an EUV-Pump NIR-Probe Configuration. *J. Phys. B* **2009**, *42* (8), 081002.
(7) Pollard, J.; Trevor, D.; Reutt, J.; Lee, Y. T.; Shirley, D. Torsional Potential and Intramolecular Dynamics in the C_2H_4 Photoelectron Spectra. *J. Chem. Phys.* **1984**, *81*, 5302−5309.
(8) Stockbauer, R.; Inghram, M. G. Threshold Photoelectron−Photoion Coincidence Mass Spectrometric Study of Ethylene and Ethylene-d_4. *J. Chem. Phys.* **1975**, *62*, 4862−4870.
(9) Merer, A.; Mulliken, R. S. Ultraviolet Spectra and Excited States of Ethylene and Its Alkyl Derivatives. *Chem. Rev.* **1969**, *69* (5), 639−656.
(10) Gelbart, W. M.; Freed, K. F.; Rice, S. A. Internal Rotation and the Breakdown of the Adiabatic Approximation: Many-Phonon Radiationless Transitions. *J. Chem. Phys.* **1970**, *52*, 2460−2473.
(11) Buenker, R.; Peyerimhoff, S.; Hsu, H. A New Interpretation for the Structure of the V−N Bands of Ethylene. *Chem. Phys. Lett.* **1971**, *11* (1), 65−70.
(12) Ben-Nun, M.; Martínez, T. J. Ab Initio Molecular Dynamics Study of *cis*−*trans* Photoisomerization in Ethylene. *Chem. Phys. Lett.* **1998**, *298* (1), 57−65.
(13) Ben-Nun, M.; Quenneville, J.; Martínez, T. J. Ab Initio Multiple Spawning: Photochemistry from First Principles Quantum Molecular Dynamics. *J. Phys. Chem. A* **2000**, *104* (22), 5161−5175.
(14) Knowles, P. J.; Werner, H.-J. An Efficient Second-Order MC-SCF Method for Long Configuration Expansions. *Chem. Phys. Lett.* **1985**, *115* (3), 259−267.
(15) Ben-Nun, M.; Martínez, T. J. Ab Initio Quantum Molecular Dynamics. *Adv. Chem. Phys.* **2002**, *121*, 439−512.
(16) Shiozaki, T.; Győrffy, W.; Celani, P.; Werner, H.-J. *Communication:* Extended Multi-State Complete Active Space Second-Order Perturbation Theory: Energy and Nuclear Gradients. *J. Chem. Phys.* **2011**, *135*, 081106.
(17) Jahn, H. A.; Teller, E. Stability of Polyatomic Molecules in Degenerate Electronic States. I. Orbital Degeneracy. *Proc. R. Soc. London, Ser. A* **1937**, *161* (905), 220−235.
(18) Maluendes, S. A.; McLean, A.; Herbst, E. New Calculations on the Ion−Molecule Processes $C_2H_2^+ + H_2 \rightarrow C_2H_3^+ + H$ and $C_2H_2^+ + H_2 \rightarrow C_2H_4^+$. *Chem. Phys. Lett.* **1994**, *217* (5−6), 571−576.
(19) van der Hart, W. J. Ab Initio Molecular Orbital Calculations on 1,2-Hydrogen Shifts in the Ethene, Allene and Propyne Radical Cations. *Int. J. Mass Spectrom.* **1995**, *151* (1), 27−34.
(20) Mori, T.; Kato, S. Dynamic Electron Correlation Effect on Conical Intersections in Photochemical Ring-Opening Reaction of Cyclohexadiene: MS-CASPT2 Study. *Chem. Phys. Lett.* **2009**, *476* (1), 97−100.
(21) Coe, J. D.; Martínez, T. J. Competitive Decay at Two- and Three-State Conical Intersections in Excited-State Intramolecular Proton Transfer. *J. Am. Chem. Soc.* **2005**, *127* (13), 4560−4561.
(22) Coe, J. D.; Martínez, T. J. Ab Initio Molecular Dynamics of Excited-State Intramolecular Proton Transfer around a Three-State Conical Intersection in Malonaldehyde. *J. Phys. Chem. A* **2006**, *110* (2), 618−630.
(23) Meyer, H.-D.; Manthe, U.; Cederbaum, L. The Multi-configurational Time-Dependent Hartree Approach. *Chem. Phys. Lett.* **1990**, *165* (1), 73−78.
(24) Krause, P.; Matsika, S. Nuclear Dynamics for a Three-State Jahn−Teller Model System. *J. Chem. Phys.* **2012**, *136*, 034110.
(25) Fuß, W. Where Does the Energy Go in fs-Relaxation? *Chem. Phys.* **2013**, *425*, 96−103.
(26) Kim, M. H.; Shen, L.; Tao, H.; Martinez, T. J.; Suits, A. G. Conformationally Controlled Chemistry: Excited-State Dynamics Dictate Ground-State Reaction. *Science* **2007**, *315* (5818), 1561−1565.
(27) Tao, H.; Shen, L.; Kim, M. H.; Suits, A. G.; Martinez, T. J. Conformationally Selective Photodissociation Dynamics of Propanal Cation. *J. Chem. Phys.* **2011**, *134* (5), 054313.